

# Performance Analysis of RIS-Assisted Large-Scale Wireless Networks Using Stochastic Geometry

Tianxiong Wang, Gaojie Chen, *Senior Member, IEEE*, Mihai-Alin Badiu,  
and Justin P. Coon, *Senior Member, IEEE*,

**Abstract**—In this paper, we investigate the performance of a reconfigurable intelligent surface (RIS) assisted large-scale network by characterizing the coverage probability and the average achievable rate using stochastic geometry. Considering the spatial correlation between transmitters (TXs) and RISs, their locations are jointly modelled by a Gauss-Poisson process (GPP). Two association strategies, i.e., nearest association and fixed association, are both discussed. For the RIS-aided transmission, the signal power distribution with a direct link is approximated by a gamma random variable using a moment matching method, and the Laplace transform of the aggregate interference power is derived in closed form. Based on these expressions, we analyze the channel hardening effect in the RIS-assisted transmission, the coverage probability, and the average achievable rate of the typical user. We derive the coverage probability expressions for the fixed association strategy and the nearest association strategy in an interference-limited scenario in closed form. Numerical results are provided to validate the analysis and illustrate the effectiveness of RIS-assisted transmission with passive beamforming in improving the system performance. Furthermore, it is also unveiled that the system performance is independent of the density of TXs with the nearest association strategy in the interference-limited scenario.

**Index Terms**—Reconfigurable intelligent surface (RIS), performance analysis, Gauss-Poisson process (GPP), stochastic geometry

## I. INTRODUCTION

Wireless connectivity and mobile data traffic have increased remarkably in the recent years [1]. As foreseen by [2], this trend will continue in the future sixth-generation (6G) wireless communication networks, which are expected to provide highly efficient and reliable wireless communication services for billions of devices. The significant demands in high data rates, reliability and massive connectivity have brought great challenges in designing wireless systems and spurred enthusiasm in developing innovative physical layer technologies. Among various potential technologies, reconfigurable intelligent surfaces (RISs) have recently been regarded as a key enabling solution owing to the theoretic and engineering development of metasurfaces [3]. Physically, RIS is a planar metasurface equipped with a smart RIS controller and a

large number of passive and low-cost elements [4]. Each reflecting element can be controlled independently by a RIS controller to adjust the phase and amplitude of the reflected signals intelligently, hence collaboratively altering the wireless propagation environment for achieving various desired purposes, such as directional signal enhancement and spatial signal nulling [5]. Compared to some related technologies, RIS has advantages in energy efficiency, low hardware cost, and convenient deployment [6]. Hence, the application of RIS is extensively investigated in different areas. RIS empowered physical layer security and RIS empowered non-orthogonal multiple access (NOMA) were studied in [7] and [8], respectively. The authors in [9] and [10] investigated the RIS-assisted UAV communications by carrying out joint trajectory and beamforming design. Besides, RIS is expected to be widely deployed in future wireless communication networks to improve communication quality and extend coverage.

Due to the attractive benefits of RIS, extensive research efforts have been devoted to the performance analysis of RIS-assisted communication systems to analyze the link-level performance gains that can be brought by integrating RISs into wireless networks. The authors in [11] derived the path loss expressions of RIS-assisted wireless networks and illustrated that the path loss is inversely proportional to the product of the distances of two cascaded links. Characterizing the small-scale fading, the authors in [12] derived the approximate outage probability, symbol error probability and average achievable rate of a RIS-assisted system over Rayleigh fading channels without phase errors by applying the central limit theorem (CLT). As a step further, the phase errors of RIS were considered in [13] and the authors proved that the composite channel of a RIS system with phase errors is Nakagami- $m$  fading. However, as shown in [14], [15], the approximation methods based on the CLT are only accurate for a very large number of elements, and the approximation errors are significant at the high transmit signal-to-noise ratio (SNR) regime. The authors in [16] proposed a moment matching approach to approximate the composite channel gain as a gamma random variable and then derive various performance metrics in closed form. The moment matching method turns out to be accurate even for a small number of elements. Following a similar method, the outage probability of a RIS-aided network with 1-bit phase shifting was derived in [17]. All the above works considered the Rayleigh fading channel model. To further investigating the general channel environment, the Nakagami- $m$  fading model was applied in [18], [19]. For example, the authors in [18] derived the outage

This research was funded in part by EPSRC grant number EP/T02612X/1. For the purpose of Open Access, the author has applied a CC BY public copyright licence to any Author Accepted Manuscript (AAM) version arising from this submission. (Corresponding author: Gaojie Chen)

T. Wang, M. A. Badiu and J. P. Coon are with the Department of Engineering Science, University of Oxford, Oxford, OX1 3PJ, U.K. (e-mail: {tianxiong.wang, mihai.badiu, justin.coon}@eng.ox.ac.uk).

G. Chen is with 5GIC & 6GIC, Institute for Communication Systems (ICS), University of Surrey, Guildford, GU2 7XH, United Kingdom (e-mail: gaojie.chen@surrey.ac.uk).

probability of a RIS aided network without phase errors over Nakagami- $m$  channels in an integral form by using the Gil-Pelaez theorem. Under the random phase-shifting scheme where the phase errors are uniformly distributed over  $(0, 2\pi)$ , the authors in [19] derived the outage probability in closed form by assuming Nakagami- $m$  fading channels. Recently, the effects of channel correlations were investigated in [20] and [21], where the outage probability of a RIS-assisted wireless network over correlated channels with random and coherent phase-shifting schemes were derived.

The aforementioned works all consider single-cell networks. However, a real RIS-assisted communication network comprises multiple transmitters, receivers and RISs, and they may share the same resource block, i.e., time and frequency. Thus, in the performance analysis of RIS-assisted communication systems, it is essential to model the RIS-assisted multi-cell network subjected to inter-cell interference. Stochastic geometry has been widely used to model and characterize the performance of large-scale wireless networks, which can provide useful performance bounds and practical insights regarding the practical wireless systems [22], [23]. Performance analysis of RIS-assisted multi-cell networks using stochastic geometry has been carried out in recent works. In [24], the authors investigated the coverage probability of a large-scale RIS-assisted millimeter wave communication network using stochastic geometry. The authors in [25] modelled the blockages as boolean line segments, and the RISs are attached to the blockages with a probability. The probability that a given user is associated with a transmitter (TX) via a RIS is derived, which shows that RISs can enlarge the coverage in a multi-cell network by providing indirect LoS paths. In [26], the authors modelled the locations of TXs and RISs as two independent homogeneous Poisson point processes (HPPP) in a multi-cell millimetre-wave (mmWave) network and derived the average achievable rate in a multi-fold integral. With a similar system setup, the authors in [27] analyzed the distributions of the signal power and interference power, respectively and derived a two-fold integral expression for the coverage probability of the typical user when it is connected with the nearest TX and RIS. RIS-assisted multi-cell NOMA networks were investigated in [28], in which the authors modelled the locations of TXs and users as HPPP and assumed the interference from other RISs that are not associated with the typical user could be ignored. The coverage probability and average achievable rate of the typical user were both derived in integral form. The performance of two different types of users, i.e., served by the TX with and without RIS-assisted transmissions, are analyzed in a more recent work [29], where the authors derived the coverage probability of the network conditioned on the proportions of the two types of users.

All the aforementioned works use independent HPPP to model the locations of TXs and RISs, because HPPP not only can model the randomly located nodes but also makes the analysis mathematically tractable [22]. However, the HPPP may not be an accurate model for large-scale RIS-assisted systems since it does not capture the spatial correlations

between TXs and RISs [30]. Since RIS is a passive device and its locations have to be appropriately designed according to the location of the TX, the locations of TXs and RISs exhibit significant spatial correlations [4]. To describe this characteristic of the large-scale RIS-assisted networks, the Gauss-Poisson process (GPP) can be applied because the GPP is a clustering process that can capture the correlations of the node locations, in which each cluster has one or two points with the spatial correlations [31].

Therefore, we use a GPP to model a large-scale RIS-assisted network to represent the spatial correlations between TXs and RISs. Furthermore, the general Nakagami- $m$  fading channel model and the RIS-assisted transmission with the direct link between the user and the TX are considered in the analysis. The main contributions of this paper are listed as follows:

- 1) To provide an accurate system-level performance analysis, we propose an analytical framework to characterize the performance of a RIS-assisted large-scale network by using stochastic geometry. The locations of UEs are modelled by an HPPP, while the locations of TXs and RISs are modelled by a cluster process GPP to characterize the spatial correlations between TXs and RISs. The channels related to the RIS are Nakagami- $m$  fading. Moreover, we consider the fixed association and nearest association strategies between the TX and the typical user in the analysis, respectively.
- 2) We obtain expressions for the coverage probability and the average achievable rate in the downlink for the typical user with the fixed and nearest association strategies. The expressions for the coverage probability have the closed forms for both association strategies in terms of elementary and/or special functions for all path loss exponents. The expressions for the average achievable rate have integral forms, which are further simplified to closed forms for certain path loss exponents.
- 3) The numerical results verify the effectiveness of the theoretical analysis, and practical insights are extracted from the analytical and numerical results. For the fixed association strategy, increasing the density of TXs and the RIS association probability will both impair the system performance due to the enhanced interference power. While for the nearest association strategy, a larger density of TXs and RIS association probability is beneficial since the typical user is more likely to be served by a closer TX with an assisting RIS. Furthermore, we prove that the coverage probability and the average achievable rate are unrelated to the density of TXs when the nearest association strategy is applied in the large transmit SNR regime.

The rest of the paper is organized as follows. The system model is introduced in Section II. The distributions of the desired signal power and the interference power for two types of association strategies are analyzed in Section III and Section IV, respectively. In Section V, the coverage probability

TABLE I  
KEY NOTATIONS

$S_0^+$	Signal power, fixed TX with assisting RIS.
$S_0^*$	Signal power, fixed TX without assisting RIS.
$I$	Total interference power.
$P_1(\bar{\gamma})$	Coverage probability, fixed TX with assisting RIS.
$P_2(\bar{\gamma})$	Coverage probability, fixed TX without assisting RIS.
$P_{c,n}(\bar{\gamma})$	Coverage probability, nearest association strategy
$\bar{P}_{c,n}(\bar{\gamma})$	Coverage probability, nearest TX, interference-limited.
$R_1$	Average rate, fixed TX with assisting RIS.
$R_2$	Average rate, fixed TX without assisting RIS.
$R_{c,n}$	Average rate, nearest association strategy

and average achievable rate are analyzed. Section VI gives the numerical results, and the paper is concluded in Section VII. For clarity, Table. I lists some key notations in this paper.

*Notations:* The expectation and variance of a random variable  $X$  are denoted as  $\mathbb{E}[X]$  and  $\text{Var}[X]$ , respectively. The cumulative distribution function (CDF) and the complementary CDF (CCDF) of a random variable  $X$  are denoted as  $F_X(x)$  and  $\bar{F}_X(x)$ , respectively.  $\mathbb{C}$  and  $\mathbb{C}^{N \times 1}$  represent the complex numbers and the  $N \times 1$  complex vectors space, respectively.  $\mathcal{CN}(\mu, \sigma^2)$  denotes the complex Gaussian distribution with mean  $\mu$  and variance  $\sigma^2$ .  $\mathcal{R}(\sigma)$  denotes the Rayleigh distribution with the scale parameter  $\sigma$ .  $\Gamma(\cdot)$ ,  $\Gamma(\cdot, \cdot)$  and  $\gamma(\cdot, \cdot)$  stand for the gamma function, upper incomplete gamma function and lower incomplete gamma function, respectively.  $\lceil \cdot \rceil$  is the rounding operation.  ${}_2F_1(\cdot, \cdot; \cdot; \cdot)$  is the hypergeometric function and  $\sim$  is the notation for the asymptotic equivalence.  $\text{erfc}(\cdot)$ ,  $\text{Ci}(\cdot)$  and  $\text{Si}(\cdot)$  denote the complementary error, cosine integral and sine integral functions, respectively.

## II. SYSTEM MODEL

This paper studies a RIS-assisted multi-cell wireless communication network with multiple single-antenna transmitters (TXs), RISs, and single-antenna user equipments (UEs)<sup>1</sup> shown in Fig. 1. The performance of the downlink communication from the TXs to UEs is analyzed. The locations of UEs are modelled by a homogeneous Poisson point process (HPPP)  $\Lambda_u$  with density  $\lambda_u$ . We consider the spatial correlations between the locations of TXs and RISs, and model the locations of TXs and RISs as a GPP  $\Lambda_c$ , which is a clustering process that can capture the correlations of the node locations [30].  $\Lambda_c$  is a Poisson cluster process where the locations of TXs are the parent process and follow a HPPP  $\Lambda_t$  with density  $\lambda_t$ . Each cluster in  $\Lambda_c$  has one or two points. If a cluster has one point, it is at the location of the parent point. Otherwise, one of them is the parent point, and the daughter

<sup>1</sup> Analysis of multi-antenna TXs and UEs will be left for our future work. Active and passive beamforming schemes should be properly designed, based on which the performance analysis can be carried out. Moreover, as shown in [27], RIS-assisted communications with single-antenna TXs is a promising cost-effective wireless communication architecture, especially in scenarios where multi-antenna systems cannot be equipped.

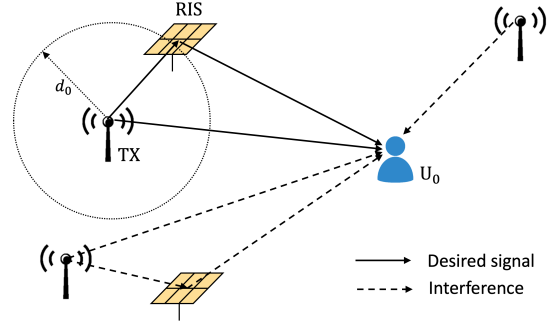


Fig. 1. System model of RIS assisted large-scale network.

point, which represents the location of an assisting RIS of the corresponding TX, is uniformly distributed on a circle with a radius  $d_0$  centred at the parent point<sup>2</sup>. The probabilities of each cluster having one or two points are  $1 - p$  and  $p$ , respectively. In other words, for a typical TX, the probability that it has an assisting RIS is  $p$ . In this paper, we study the system where each TX can be served by one RIS at most. Performance analysis on the system where each TX has more than one assisting RIS remains a critical question for the future work. In that case, more sophisticated PCP models are required to jointly model the locations of TXs and RISs. For notational simplicity, we denote the cluster processes with one point and two points as  $\Lambda_1$  and  $\Lambda_2$ , respectively. Based on the definition of GPP, we have

$$\Lambda_c = \Lambda_1 \cup \Lambda_2. \quad (1)$$

Furthermore, the parent and daughter point processes of the clusters with two points are respectively denoted as  $\Lambda_2^{(P)}$  and  $\Lambda_2^{(D)}$  such that

$$\Lambda_2 = \Lambda_2^{(P)} \cup \Lambda_2^{(D)}. \quad (2)$$

Since the locations of UEs are assumed to follow a HPPP, we can randomly select a typical UE  $U_0$  from  $\Lambda_u$  and fix it at the origin of the considered plane. As per Slivnyak's theorem, the performance of  $U_0$  represents the average UE performance.

### A. Channel Model

It is assumed that each RIS has  $N$  elements and can perform continuous phase adjustment to increase the composite channel gain of its serving UE, which gives an upper bound on the system performance [32]. Furthermore, as proved in [33], [34], only two-bit phase shifting leads to the performance close to upper bound in practice. The transmit power of each TX is  $P$ . The normalized small scale fading of the  $T_i$ - $U_0$  channel is denoted as  $g_i \in \mathbb{C}$  where  $i \in \Lambda_t$ . The direct links between TXs and UEs are assumed to be Rayleigh fading channels, i.e.,  $|g_i| \sim \mathcal{R}(\sqrt{2}/2)$ . The Rayleigh fading model

<sup>2</sup>In this paper, we consider the standard GPP where  $d_0$  is fixed for clarity. The proposed results can be easily extended to the generalized GPP model by averaging the derived coverage probability and average achievable rate over the distribution of  $d_0$ .

applies to rich scattering urban environments and stable LoS paths do not exist between TXs and UEs [34]. The path loss of the direct link  $T_i-U_0$  can be expressed as

$$\eta_{g,i} = C_d d_{g,i}^{-\alpha}, \quad (3)$$

where  $d_{g,i}$  is the distance of the  $T_i-U_0$  channel;  $C_d$  is the path loss per unit distance of the direct link;  $\alpha$  is the path loss exponent. Similar to [35]–[37], it is assumed that the horizontal distances of different channels are much larger than the vertical distances and the heights of TXs, RISs and UEs are ignored.

It is assumed that each RIS receives the signal from its associated TX and the signals from other TXs impinging on the RIS can be ignored<sup>3</sup>. For  $T_j$ ,  $j \in \Lambda_2^{(P)}$  that has an assisting RIS  $R_{j'}$ ,  $j' \in \Lambda_2^{(D)}$ , the normalized small scale fading of the  $T_j-R_{j'}$  and  $R_{j'}-U_0$  channels are denoted as  $\mathbf{h}_j = (h_{j,1}, \dots, h_{j,N})^T \in \mathbb{C}^{N \times 1}$ , and  $\mathbf{r}_j = (r_{j,1}, \dots, r_{j,N})^T \in \mathbb{C}^{N \times 1}$ , respectively.  $T_j$  and  $R_{j'}$  are the parent and daughter points in the same two-point cluster. RISs operate in the far field of both TXs and UEs. We assume the reflected links associated with RISs are Nakagami- $m$  fading channels. To be specific,  $|h_{j,n}| \sim \text{Nakagami}(m_h, 1)$  and  $|r_{j,n}| \sim \text{Nakagami}(m_r, 1)$ , where  $n \in \{1, \dots, N\}$ .  $m_h$  and  $m_r$  are the shape parameters of  $|h_{j,n}|$  and  $|r_{j,n}|$ , respectively. It is worth noting that the Nakagami- $m$  is a general distribution to model many different types of channel fading by adjusting the shape parameter, e.g., the Nakagami- $m$  distribution is equivalent to the Rayleigh distribution if the shape parameter equals to one [38]. The path loss of the reflected path  $T_j-R_{j'}-U_0$  can be expressed as

$$\eta_{h,j} = C_r (d_0 d_{r,j})^{-\alpha}, \quad (4)$$

where  $d_{r,j}$  is the distance of the  $R_{j'}-U_0$  channel;  $C_r$  is the path loss per unit distance of the reflected link.

### B. Signal Model

The received signal at  $U_0$  depends on whether its associated TX  $T_0$  has an assisting RIS or not. If  $T_0$  has an assisting RIS, the received signal at  $U_0$  can be expressed as

$$y_0^+ = (\sqrt{\eta_{g,0}}g_0 + \sqrt{\eta_{h,0}}\mathbf{h}_0^T \Phi_0 \mathbf{r}_0) \sqrt{P}s_0 + \tilde{I} + n_0, \quad (5)$$

where

$$\begin{aligned} \tilde{I} = & \sum_{k \in \Lambda_t \setminus \{0\}} (1 - b_k) \sqrt{\eta_{g,k}} \bar{P} g_k s_k \\ & + b_k (\sqrt{\eta_{g,k}} g_k + \sqrt{\eta_{h,k}} \mathbf{h}_k^T \Phi_k \mathbf{r}_k) \sqrt{P} s_k, \end{aligned} \quad (6)$$

representing the interference from all other TXs.  $\Phi_k = \text{diag}(e^{j\phi_{k,1}}, \dots, e^{j\phi_{k,N}})$  is the phase shifting matrix of  $R_{k'}$ , and  $R_{k'}$  is the assisting RIS of  $T_k$  in a two-point cluster;  $b_k \in \{0, 1\}$  represents if  $T_k$  is without or with an assisting RIS, respectively;  $s_k$  is the unit power transmit symbol from  $T_k$ , satisfying  $\mathbb{E}[s_k^2] = 1$  and  $\mathbb{E}[s_k s_l] = 0$  for  $k \neq l$ ;  $n_0 \sim$

<sup>3</sup>In this paper, we consider the spatial correlation between the locations of TXs and RISs. This assumption is particularly valid when the distances among different TXs are significantly larger than the distance between a TX and its associated RIS. A similar assumption is also applied in [28], [29].

$\mathcal{CN}(0, \sigma_0^2)$  is the additive white Gaussian noise (AWGN) with zero mean and variance  $\sigma_0^2$ . If  $T_0$  does not have an assisting RIS, the received signal at  $U_0$  can be expressed as

$$y_0^* = \sqrt{\eta_{g,0}} \bar{P} g_0 s_0 + \tilde{I} + n_0. \quad (7)$$

If  $T_0$  has an assisting RIS, the phase shifts of  $R_0$  should be adjusted to align the phases of the reflected paths to the phase of the direct link, i.e.,

$$\phi_{0,n} = -\arg(h_{0,n}) - \arg(r_{0,n}) + \arg(g_0). \quad (8)$$

On the other hand, the phases of the composite channels  $T_l-R_{l'}-U_0$ ,  $l \in \Lambda_2^{(P)} \setminus \{0\}$  can be regarded as uniformly distributed over  $[-\pi, \pi)$ . Following the above discussions, (5) can be written as

$$\begin{aligned} y_0^+ = & \left( \sqrt{\eta_{g,0}}|g_0| + \sqrt{\eta_{h,0}} \sum_{n=1}^N |h_{0,n}| |r_{0,n}| \right) e^{j \arg(g_0)} \sqrt{P} s_0 \\ & + \sqrt{P} \tilde{I} + n_0, \end{aligned} \quad (9)$$

where

$$\tilde{I} = \sum_{k \in \Lambda_t \setminus \{0\}} b_k \tilde{I}_{1,k} + (1 - b_k) \tilde{I}_{2,k}; \quad (10a)$$

$$\tilde{I}_{1,k} = \left( \sqrt{\eta_{g,k}} g_k + \sqrt{\eta_{h,k}} \sum_{n=1}^N |h_{k,n}| |r_{k,n}| e^{j\theta_{k,n}} \right) s_k; \quad (10b)$$

$$\tilde{I}_{2,k} = \sqrt{\eta_{g,k}} g_k s_k, \quad (10c)$$

and  $\theta_{k,n}$  is uniformly distributed over  $[-\pi, \pi)$ .

Then, we will give the SINR of  $U_0$  at different association strategies as follows:

- 1) With the fixed association strategy, the SINR of  $U_0$  with an assisting RIS is given by

$$\gamma_0^+ = \frac{S_0^+}{I + \gamma_t^{-1}}, \quad (11)$$

where  $\gamma_t = P/\sigma_0^2$ . The signal power  $S_0^+$  is

$$S_0^+ = \left( \sqrt{\eta_{g,0}}|g_0| + \sqrt{\eta_{h,0}} \sum_{n=1}^N |h_{0,n}| |r_{0,n}| \right)^2. \quad (12)$$

The interference power is

$$I = |\tilde{I}|^2 = \sum_{k \in \Lambda_t \setminus \{0\}} b_k I_{1,k} + (1 - b_k) I_{2,k}, \quad (13)$$

in which

$$I_{1,k} = |\tilde{I}_{1,k}|^2 \quad (14a)$$

$$= \left| \sqrt{\eta_{g,k}} g_k + \sqrt{\eta_{h,k}} \sum_{n=1}^N |h_{k,n}| |r_{k,n}| e^{j\theta_{k,n}} \right|^2,$$

$$I_{2,k} = |\tilde{I}_{2,k}|^2 = |\sqrt{\eta_{g,k}} g_k|^2. \quad (14b)$$

- 2) With the fixed association strategy, the SINR of  $T_0$  without an assisting RIS can be given by

$$\gamma_0^* = \frac{S_0^*}{I + \gamma_t^{-1}}, \quad (15)$$

where

$$S_0^* = \eta_{g,0} |g_0|^2. \quad (16)$$

3) With the nearest association strategy, the SINR of  $U_0$  is given by<sup>4</sup>

$$\gamma_0 = \begin{cases} \gamma_0^+, & \text{w.p. } p, \\ \gamma_0^*, & \text{w.p. } 1-p, \end{cases} \quad (17)$$

### C. Performance Metrics

In this paper, we will analyze the coverage probability and average achievable rate of the typical user  $U_0$ .

1) *Coverage Probability*: Coverage probability is defined as the probability that the received SINR is larger than a threshold, i.e.,

$$P_c(\bar{\gamma}) = \mathbb{P}(\gamma > \bar{\gamma}), \quad (18)$$

where  $\gamma \in \{\gamma_0^+, \gamma_0^*, \gamma_0\}$ ;  $\bar{\gamma}$  is the coverage SINR threshold.

2) *Average Achievable Rate*: The average achievable rate of the typical user is defined as

$$R = \int_0^\infty \log_2(1+x) f_\gamma(x) dx, \quad (19)$$

where  $f_\gamma(x)$  is the PDF of  $\gamma$ .

## III. SIGNAL POWER ANALYSIS

In this section, we characterize the signal power distributions with and without RIS reflect beamforming, which are denoted as  $S_0^+$  and  $S_0^*$ , respectively.

### A. Distribution with RIS-Assisted Transmission

The received signal power with RIS-assisted transmission  $S_0^+$  can be rewritten as

$$S_0^+ = (\sqrt{\eta_{g,0}} |g_0| + \sqrt{\eta_{h,0}} S_r)^2, \quad (20)$$

where

$$S_r = \sum_{n=1}^N |h_{0,n}| |r_{0,n}|, \quad (21)$$

which is the sum of the products of Nakagami- $m$  random variables. The exact distribution of  $S_r$  cannot be obtained in closed form. Hence, we propose a moment matching method based on gamma distribution to fit the distribution of  $S_r$ .

<sup>4</sup> $\gamma_0$  is a function of the distance between  $T_i$  and  $U_0$ ,  $i \in \Lambda_t$ , i.e.,  $d_{g,i}$ . With the nearest association strategy,  $U_0$  is associated with the TX with the minimum  $d_{g,i}$ .

Since  $|h_{0,n}|$  and  $|r_{0,n}|$ ,  $n \in \{1, \dots, N\}$  are independent and identically distributed (i.i.d.) Nakagami- $m$  random variables, the mean and second order raw moment of  $S_r$  are derived as:

$$\begin{aligned} \mathbb{E}[S_r] &= \sum_{n=1}^N \mathbb{E}[|h_{0,n}|] \mathbb{E}[|r_{0,n}|] \\ &= N \frac{\Gamma(m_h + \frac{1}{2})}{\Gamma(m_h)} \frac{\Gamma(m_r + \frac{1}{2})}{\Gamma(m_r)} \left( \frac{1}{m_h m_r} \right)^{\frac{1}{2}}, \end{aligned} \quad (22a)$$

$$\begin{aligned} \mathbb{E}[S_r^2] &= \mathbb{E} \left[ \sum_{n=1}^N |h_{0,n}|^2 |r_{0,n}|^2 \right] \\ &\quad + 2 \mathbb{E} \left[ \sum_{n=1}^{N-1} \sum_{i=n+1}^N |h_{0,n}| |r_{0,n}| |h_{0,i}| |r_{0,i}| \right] \\ &= N + N(N-1) \times \\ &\quad \left( \frac{\Gamma(m_h + \frac{1}{2})}{\Gamma(m_h)} \frac{\Gamma(m_r + \frac{1}{2})}{\Gamma(m_r)} \right)^2 \frac{1}{m_h m_r}. \end{aligned} \quad (22b)$$

Hence,  $S_r$  can be approximated by a gamma random variable with shape and scale parameters:

$$\kappa_r = \frac{\mathbb{E}^2[S_r]}{\mathbb{E}[S_r^2] - \mathbb{E}^2[S_r]}, \quad (23a)$$

$$\omega_r = \frac{\mathbb{E}[S_r^2] - \mathbb{E}^2[S_r]}{\mathbb{E}[S_r]}. \quad (23b)$$

The moment matching approach can be applied to fit the distribution of  $S_0^+$ . Then the mean and second order moment of  $S_0^+$  can be derived as

$$\mathbb{E}[S_0^+] = \eta_{g,0} \chi_1, \quad (24a)$$

$$\mathbb{E}[(S_0^+)^2] = \eta_{g,0}^2 \chi_2, \quad (24b)$$

where

$$\beta = \sqrt{\eta_{h,0}/\eta_{g,0}}, \quad (25a)$$

$$\chi_1 = \mu_2^g + 2\beta\mu_1^g\mu_1^\varsigma + \beta^2\mu_2^\varsigma, \quad (25b)$$

$$\chi_2 = \mu_4^g + 4\beta\mu_3^g\mu_1^\varsigma + 6\beta^2\mu_2^g\mu_2^\varsigma + 4\beta^3\mu_1^g\mu_3^\varsigma + \beta^4\mu_4^\varsigma. \quad (25c)$$

$\mu_q^\epsilon$ ,  $\epsilon \in \{g, \varsigma\}$ ,  $q \in \{1, 2, 3, 4\}$  denotes the  $q$ th order raw moment of  $|g_0|$  and  $S_r$ , respectively. Since  $|g_0| \sim \mathcal{R}(\sqrt{2}/2)$  and  $S_r$  has been fitted by a gamma random variable,  $\mu_q^g$  and  $\mu_q^\varsigma$  are given by

$$\mu_q^g = \Gamma\left(1 + \frac{1}{2}q\right), \quad (26a)$$

$$\mu_q^\varsigma = \omega_r^q \frac{\Gamma(q + \kappa_r)}{\Gamma(\kappa_r)}. \quad (26b)$$

Therefore,  $S_0^+$  can be approximated by a gamma random variable with shape and scale parameters as

$$\kappa_s = \frac{\chi_1^2}{\chi_2 - \chi_1^2}, \quad (27a)$$

$$\omega_s = \eta_{g,0} \bar{\chi} = \eta_{g,0} \frac{\chi_2 - \chi_1^2}{\chi_1}. \quad (27b)$$

Furthermore, the approximate probability density function (PDF) and cumulative distribution function (CDF) of  $S_0^+$  are given by

$$f_{S_0^+}(x) = \frac{x^{\kappa_s-1} \exp(-x/\omega_s)}{\Gamma(\kappa_s) \omega_s^{\kappa_s}}, \quad (28a)$$

$$F_{S_0^+}(x) = \frac{\gamma(\kappa_s, x/\omega_s)}{\Gamma(\kappa_s)}. \quad (28b)$$

Now, we investigate the channel hardening effect in the proposed system for a large number of elements. The coefficient of variation, i.e., the ratio of the standard deviation to the mean, is summarized in the following corollary.

**Corollary 1.** *For a large number of RIS elements, the coefficient of variation of  $S_0^+$  satisfies the asymptotic property:*

$$\nu_s = O\left(\frac{1}{\sqrt{N}}\right), \quad N \rightarrow \infty. \quad (29)$$

*Proof:* See Appendix A.  $\square$

**Remark 1.** *As introduced in [27], the channel hardening effect refers to the fact that the variation of the signal power around the mean power decreases with the increase of the number of elements. Since the coefficient of variation shows the variability extent of a random variable in relation to its mean value, it can be learned from Corollary 1 that increasing the number of elements will lead to less variability of  $S_0^+$  around its mean value. Hence, the channel hardening effect appears. Due to the channel hardening effect, the variation of the channel is averaged out and the overhead of frequent channel estimation is reduced.*

#### B. Distribution without RIS Beamforming

Since  $|g_0| \sim \mathcal{R}(\sqrt{2}/2)$ ,  $S_0^*$  follows the exponential distribution with the distribution parameter  $\zeta_g = 1/\eta_{g,0}$ . The PDF and CDF of  $S_0^*$  are respectively given by

$$f_{S_0^*}(x) = \frac{1}{\eta_{g,0}} e^{-\frac{x}{\eta_{g,0}}}, \quad (30a)$$

$$F_{S_0^*}(x) = 1 - e^{-\frac{x}{\eta_{g,0}}}. \quad (30b)$$

### IV. INTERFERENCE POWER ANALYSIS

In this section, the interference power  $I$  is analyzed. Referring to (13), (14a) and (14b), we first characterize the distributions of  $I_{1,k}$  and  $I_{2,k}$ , respectively. Then, the Laplace transform of  $I$  is computed which is used in analyzing the coverage probability and the average achievable rate of the typical user.

#### A. Interference Power Distribution Analysis

1) *Interference from TX with Assisting RIS:* The interference power from a TX with an assisting RIS  $I_{1,k}$  is rewritten by

$$I_{1,k} = \left| \sqrt{\eta_{g,k}} g_k + \sqrt{\eta_{h,k}} I_{r,k} \right|^2, \quad (31)$$

where

$$I_{r,k} = \sum_{n=1}^N |h_{k,n}| |r_{k,n}| e^{j\theta_{k,n}}. \quad (32)$$

Then, the distribution of  $I_{r,k}$  is analyzed. Since  $\theta_{k,n}$  is uniformly distributed over  $[-\pi, \pi)$ , the expectation and variance of  $|h_{k,n}| |r_{k,n}| \cos(\theta_{k,n})$  and  $|h_{k,n}| |r_{k,n}| \sin(\theta_{k,n})$  can be obtained as

$$\begin{aligned} \mathbb{E}[|h_{k,n}| |r_{k,n}| \cos(\theta_{k,n})] &= \mathbb{E}[|h_{k,n}| |r_{k,n}| \sin(\theta_{k,n})] = 0, \\ \text{Var}[|h_{k,n}| |r_{k,n}| \cos(\theta_{k,n})] &= \text{Var}[|h_{k,n}| |r_{k,n}| \sin(\theta_{k,n})] = \frac{1}{2}. \end{aligned}$$

Further, it can be proved that  $|h_{k,n}| |r_{k,n}| \cos(\varphi_{k,n})$  and  $|h_{k,n}| |r_{k,n}| \sin(\varphi_{k,n})$  are uncorrelated with each other, since

$$\begin{aligned} \mathbb{E}[|h_{k,n}|^2 |r_{k,n}|^2 \cos(\varphi_{k,n}) \sin(\varphi_{k,n})] \\ = \mathbb{E}[|h_{k,n}| |r_{k,n}| \cos(\theta_{k,n})] \mathbb{E}[|h_{k,n}| |r_{k,n}| \sin(\theta_{k,n})] = 0. \end{aligned} \quad (33)$$

Using the central limit theorem, for a large number of elements  $N$ ,  $I_{r,k}$  follows the circularly symmetric complex Gaussian (CSCG) distribution

$$I_{r,k} \sim \mathcal{CN}(0, N). \quad (34)$$

Since  $g_k$  follows the CSCG distribution, i.e.,  $g_k \sim \mathcal{CN}(0, 1)$ , it can be learned that

$$\sqrt{\eta_{g,k}} g_k + \sqrt{\eta_{h,k}} I_{r,k} \sim \mathcal{CN}(0, \eta_{g,k} + N\eta_{h,k}). \quad (35)$$

Thus,  $I_{1,k}$  follows the exponential distribution with the distribution parameter

$$\zeta_k = \frac{1}{\eta_{g,k} + N\eta_{h,k}}. \quad (36)$$

**Remark 2.** *Different from the moment matching method based on the gamma distribution used in the analysis of the signal power distribution, the CLT method is used in the analysis of the interference power. There are several reasons for this change. First, due to the RIS-assisted transmission,  $S_r$  is the sum of positive random variables. Approximating  $S_r$  with the gamma distribution is more reasonable because a gamma random variable is also positive. However, the support of a Gaussian random variable is the set of reals. Hence, using the CLT to analyze  $S_r$  will lead to significant errors especially in the lower tail of the distribution. This point is also illustrated in [15]. In contrast to  $S_r$ , the phase of each term in  $I_{r,k}$  is uniformly distributed over  $[-\pi, \pi)$ . Therefore, the real and imaginary parts of  $I_{r,k}$  are both supported on the real line, and using the CLT to approximate  $I_{r,k}$  as a CSCG random variable is more accurate.*

**Remark 3.** *With the CLT, the PDF and CDF of  $I_{1,k}$  is unrelated to the scale parameter of the Nakagami- $m$  distribution.*

2) *Interference from TX without Assisting RIS*: As defined in (14a), Since  $|g_k| \sim \mathcal{R}(\sqrt{2}/2)$ ,  $I_{2,k}$  follows the exponential distribution with the distribution parameter  $\zeta_{g,k} = 1/\eta_{g,k}$ . The PDF and CDF of  $I_{2,k}$  are given by

$$f_{I_{2,k}}(x) = \frac{1}{\eta_{g,k}} e^{-\frac{x}{\eta_{g,k}}}, \quad (37a)$$

$$F_{I_{2,k}}(x) = 1 - e^{-\frac{x}{\eta_{g,k}}}. \quad (37b)$$

### B. Laplace Transform of the Interference Power

The Laplace transform of the interference power is useful in the analysis of the coverage probability in the next section. Hence, the Laplace transform of the interference power with the fixed and nearest association strategies can be obtained as follows.

1) *Fixed Association Strategy*: If  $U_0$  is associated with a TX at a fixed location, i.e.,  $d_{g,0}$  is a fixed value, the Laplace transform of the interference power is summarized in the following proposition.

**Proposition 1.** *The Laplace transform of the interference power  $I$  with the fixed association strategy is*

$$\mathcal{L}_{I,f}(s) = E_{f,1}(s) E_{f,2}(s), \quad (38)$$

where

$$E_{f,1}(s) = \exp\left(-\frac{2\pi^2 \lambda_t p \csc\left(\frac{2\pi}{\alpha}\right) (e_1 s)^{\frac{2}{\alpha}}}{\alpha}\right), \quad (39a)$$

$$E_{f,2}(s) = \exp\left(-\frac{2\pi^2 \lambda_t (1-p) \csc\left(\frac{2\pi}{\alpha}\right) (C_d s)^{\frac{2}{\alpha}}}{\alpha}\right), \quad (39b)$$

$$e_1 = (C_d + N C_r d_0^{-\alpha}). \quad (39c)$$

*Proof*: See Appendix B.  $\square$

2) *Nearest Association Strategy*: If  $U_0$  is associated with the nearest TX, the Laplace transform of the interference power is given in the following proposition.

**Proposition 2.** *The Laplace transform of the interference power  $I$  with nearest association strategy is*

$$\mathcal{L}_{I,n}(s) = E_{n,1}(s) E_{n,2}(s), \quad (40)$$

where  $E_{n,1}(s)$  and  $E_{n,2}(s)$  are given in (41a) and (41b) at the top of next page, respectively.  $d_{g,0}$  is the distance between  $U_0$  and the associated TX that is closest to  $U_0$ .

*Proof*: The proof is similar to the Proposition 1 by changing lower limit of the integration to  $d_{g,0}$ , as given in (42) at the top of next page.  $\square$

## V. PERFORMANCE ANALYSIS

In this section, we analyze the coverage probability and the average achievable rate of the typical user with the fixed and nearest association strategies.

### A. Coverage Probability Analysis

1) *Fixed Association with Assisting RIS*: The main result is concluded in the following proposition.

**Proposition 3.** *If  $U_0$  is associated with a TX at a fixed location and the TX has an assisting RIS, the coverage probability of  $U_0$  is*

$$P_1(\bar{\gamma}) = \sum_{i=0}^{\hat{\kappa}_s-1} \frac{(-1)^i}{i!} \left[ \frac{\partial^i}{\partial s^i} \exp(V(s)) \right]_{s=1}, \quad (43)$$

where

$$\hat{\kappa}_s = \lfloor \kappa_s \rfloor, \quad (44a)$$

$$V(s) = -\frac{s\bar{\gamma}}{\omega_s} \gamma_t^{-1} - \frac{2\pi^2 \lambda_t p \csc\left(\frac{2\pi}{\alpha}\right) \left(\frac{e_1 \bar{\gamma}}{\omega_s} s\right)^{\frac{2}{\alpha}}}{\alpha} - \frac{2\pi^2 \lambda_t (1-p) \csc\left(\frac{2\pi}{\alpha}\right) \left(\frac{C_d \bar{\gamma}}{\omega_s} s\right)^{\frac{2}{\alpha}}}{\alpha}. \quad (44b)$$

*Proof*: See Appendix C.  $\square$

**Remark 4.** *We take another step to round  $\kappa_s$  to its nearest positive integer. We will study errors introduced by the rounding operation through simulations.*

2) *Fixed Association without Assisting RIS*: If the associated TX does not have an assisting RIS, the coverage probability is derived in the following proposition.

**Proposition 4.** *If  $U_0$  is associated with a TX at a fixed location and the TX does not have an assisting RIS, the coverage probability of  $U_0$  is*

$$P_2(\bar{\gamma}) = \exp\left(-\frac{\bar{\gamma}}{\eta_{g,0}} \gamma_t^{-1} - \frac{2\pi^2 \lambda_t p \csc\left(\frac{2\pi}{\alpha}\right) \left(\frac{e_1 \bar{\gamma}}{\eta_{g,0}}\right)^{\frac{2}{\alpha}}}{\alpha} - \frac{2\pi^2 \lambda_t (1-p) \csc\left(\frac{2\pi}{\alpha}\right) \left(\frac{C_d \bar{\gamma}}{\eta_{g,0}}\right)^{\frac{2}{\alpha}}}{\alpha}\right). \quad (45)$$

*Proof*: See Appendix D.  $\square$

**Remark 5.** *As can be seen from (45), increasing the density of TXs will lead to lower coverage probability due to the increased interference power.*

3) *Nearest Association Strategy*: If  $U_0$  is associated with the nearest TX, the PDF of  $d_{g,0}$  is given by

$$f_{d_{g,0}}(x) = 2\pi \lambda_t x e^{-\lambda_t \pi x^2}. \quad (46)$$

Then, the coverage probability of  $U_0$  is given in the following proposition

$$E_{n,1}(s) = \exp \left( \pi \lambda_t p d_{g,0}^2 \left( 1 - {}_2F_1 \left( 1, -\frac{2}{\alpha}; 1 - \frac{2}{\alpha}; -e_1 d_{g,0}^{-\alpha} s \right) \right) \right), \quad (41a)$$

$$E_{n,2}(s) = \exp \left( \pi \lambda_t (1-p) d_{g,0}^2 \left( 1 - {}_2F_1 \left( 1, -\frac{2}{\alpha}; 1 - \frac{2}{\alpha}; -C_d d_{g,0}^{-\alpha} s \right) \right) \right). \quad (41b)$$

$$\mathcal{L}_{I,n}(s) = \exp \left( 2\pi \lambda_t \int_{d_{g,0}}^{\infty} \left( \frac{p}{1 + s e_1 r^{-\alpha}} + \frac{1-p}{1 + s C_d r^{-\alpha}} - 1 \right) r dr \right) = E_{n,1}(s) E_{n,2}(s). \quad (42)$$

**Proposition 5.** *With the nearest association strategy, the coverage probability of  $U_0$  is given in an integral form as*

$$P_{c,n}(\bar{\gamma}) = p \int_0^{\infty} q^+(r) f_{d_{g,0}}(r) dr + (1-p) \int_0^{\infty} q^*(r) f_{d_{g,0}}(r) dr, \quad (47)$$

where

$$q^+(r) = \sum_{i=0}^{\hat{\kappa}_s-1} \frac{(-1)^i}{i!} \left[ \frac{\partial^i}{\partial s^i} \exp(W(s, r)) \right]_{s=1}, \quad (48a)$$

$$W(s, r) = -\frac{\bar{\gamma} \gamma_t^{-1}}{C_d \bar{\chi}} r^{\alpha} s + \pi \lambda_t r^2 \quad (48b)$$

$$- \pi \lambda_t p r^2 {}_2F_1 \left( 1, -\frac{2}{\alpha}; 1 - \frac{2}{\alpha}; -\frac{e_1 \bar{\gamma}}{C_d \bar{\chi}} s \right) - \pi \lambda_t (1-p) r^2 {}_2F_1 \left( 1, -\frac{2}{\alpha}; 1 - \frac{2}{\alpha}; -\frac{\bar{\gamma}}{\bar{\chi}} s \right),$$

$$q^*(r) = \exp \left( -\frac{\bar{\gamma} \gamma_t^{-1}}{C_d} r^{\alpha} + \pi \lambda_t r^2 \right) \quad (48c)$$

$$- \pi \lambda_t p r^2 {}_2F_1 \left( 1, -\frac{2}{\alpha}; 1 - \frac{2}{\alpha}; -\frac{e_1 \bar{\gamma}}{C_d} \right) - \pi \lambda_t (1-p) r^2 {}_2F_1 \left( 1, -\frac{2}{\alpha}; 1 - \frac{2}{\alpha}; -\bar{\gamma} \right).$$

*Proof:* See Appendix E.  $\square$

For  $\alpha = 4$ , the above expression in Proposition 5 can be further simplified, which is summarized in the following Corollary.

**Corollary 2.** *For  $\alpha = 4$ , the coverage probability of  $U_0$  with the nearest association strategy is given in closed form as*

$$P_{c,n}(\bar{\gamma}) = \frac{\pi \lambda_t p}{2} \sum_{i=0}^{\hat{\kappa}_s-1} \frac{(-1)^i}{i!} \left[ \frac{\partial^i}{\partial s^i} X^+(s) \right]_{s=1} + \frac{\pi \lambda_t (1-p)}{2} X^*, \quad (49)$$

$$X^+(s) = \frac{\sqrt{\pi} \exp \left( \frac{X_2^2(s)}{4X_1(s)} \right) \operatorname{erfc} \left( \frac{X_2(s)}{2\sqrt{X_1(s)}} \right)}{\sqrt{X_1(s)}}, \quad (50a)$$

$$X_1(s) = \frac{\bar{\gamma} \gamma_t^{-1}}{C_d \bar{\chi}} s, \quad (50b)$$

$$X_2(s) = \pi \lambda_t p {}_2F_1 \left( 1, -\frac{1}{2}; \frac{1}{2}; -\frac{e_1 \bar{\gamma}}{C_d \bar{\chi}} s \right) + \pi \lambda_t (1-p) {}_2F_1 \left( 1, -\frac{1}{2}; \frac{1}{2}; -\frac{\bar{\gamma}}{\bar{\chi}} s \right), \quad (50c)$$

$$X^* = \frac{\sqrt{\pi} \exp \left( \frac{X_4^2}{4X_3} \right) \operatorname{erfc} \left( \frac{X_4}{2\sqrt{X_3}} \right)}{\sqrt{X_3}}, \quad (50d)$$

$$X_3 = \frac{\bar{\gamma} \gamma_t^{-1}}{C_d}, \quad (50e)$$

$$X_4 = \pi \lambda_t p {}_2F_1 \left( 1, -\frac{1}{2}; \frac{1}{2}; -\frac{e_1 \bar{\gamma}}{C_d} \right) + \pi \lambda_t (1-p) {}_2F_1 \left( 1, -\frac{1}{2}; \frac{1}{2}; -\bar{\gamma} \right). \quad (50f)$$

*Proof:* It can be proved by using the interchangeable property of differentiation and integration.  $\square$

Then, we consider the interference-limited case where the noise power is negligible compared to the transmit power  $P$ , such that  $\gamma_t^{-1} \approx 0$ . In this case, the closed form outage probability expression can be derived, which is summarized in the following Proposition.

**Proposition 6.** *If  $P \gg \sigma_0^2$ , the coverage probability of  $U_0$  can be expressed as*

$$\tilde{P}_{c,n}(\bar{\gamma}) = p \sum_{i=0}^{\hat{\kappa}_s-1} \frac{(-1)^i}{i!} \left[ \frac{\partial^i}{\partial s^i} (Y_1(s))^{-1} \right]_{s=1} + (1-p)(Y_2)^{-1} \quad (51)$$



where

$$Y_1(s) = p {}_2F_1\left(1, -\frac{2}{\alpha}; 1 - \frac{2}{\alpha}; -\frac{e_1\bar{\gamma}}{C_d\bar{\chi}}s\right) + (1-p) {}_2F_1\left(1, -\frac{2}{\alpha}; 1 - \frac{2}{\alpha}; -\frac{\bar{\gamma}}{\bar{\chi}}s\right), \quad (52a)$$

$$Y_2 = p {}_2F_1\left(1, -\frac{2}{\alpha}; 1 - \frac{2}{\alpha}; -\frac{e_1\bar{\gamma}}{C_d}s\right) + (1-p) {}_2F_1\left(1, -\frac{2}{\alpha}; 1 - \frac{2}{\alpha}; -\bar{\gamma}\right). \quad (52b)$$

*Proof:* As  $\gamma_t^{-1} \rightarrow 0$ ,  $W(s)$  and  $q^*(r)$  defined in Proposition 5 can be simplified as

$$W(s, r) = \pi\lambda_t r^2 - \pi\lambda_t p r^2 {}_2F_1\left(1, -\frac{2}{\alpha}; 1 - \frac{2}{\alpha}; -\frac{e_1\bar{\gamma}}{C_d\bar{\chi}}s\right) - \pi\lambda_t (1-p) r^2 {}_2F_1\left(1, -\frac{2}{\alpha}; 1 - \frac{2}{\alpha}; -\frac{\bar{\gamma}}{\bar{\chi}}s\right), \quad (53a)$$

$$q^*(r) = \exp\left(\pi\lambda_t r^2 - \pi\lambda_t p r^2 {}_2F_1\left(1, -\frac{2}{\alpha}; 1 - \frac{2}{\alpha}; -\frac{e_1\bar{\gamma}}{C_d}\right) - \pi\lambda_t (1-p) r^2 {}_2F_1\left(1, -\frac{2}{\alpha}; 1 - \frac{2}{\alpha}; -\bar{\gamma}\right)\right). \quad (53b)$$

Recalling the definition of  $P_{c,n}(\bar{\gamma})$  in Proposition 5 and using the interchangeable property of integration and differentiation, we can obtain the result in Proposition 6.  $\square$

**Remark 6.** It turns out the coverage probability of  $U_0$  does not depend on  $\lambda_t$  in the interference-limited scenario. With the nearest association strategy, increasing the density of TXs will help  $U_0$  connect with a closer TX. On the other hand, the larger density of TXs will lead to enhanced interference. Proposition 6 shows that these two effects can perfectly offset each other. This point will be further illustrated by numerical results in Sec. VI.

### B. Average Achievable Rate Analysis

The average achievable rate of the typical user can be derived from the coverage probability expression. A lemma regarding the relationship between the average achievable rate and the coverage probability is first provided.

**Lemma 1.** If the coverage probability of the typical user is  $P_c(\bar{\gamma})$ , where  $\bar{\gamma}$  is the coverage SINR threshold, the average achievable rate of the typical user can be written as

$$R = \frac{1}{\ln(2)} \int_0^\infty \frac{P_c(x)}{1+x} dx. \quad (54)$$

*Proof:* See Appendix F.  $\square$

**Corollary 3.** For the fixed association strategy, the average achievable rate of  $U_0$  with and without an assisting RIS can be respectively given as

$$R_1 = \frac{1}{\ln(2)} \int_0^\infty \frac{P_1(x)}{1+x} dx, \quad (55a)$$

$$R_2 = \frac{1}{\ln(2)} \int_0^\infty \frac{P_2(x)}{1+x} dx, \quad (55b)$$

where  $P_1(x)$  and  $P_2(x)$  are defined in Proposition 3 and Proposition 4, respectively.

If  $\alpha = 4$ ,  $R_1$  and  $R_2$  in the interference-limited scenario can be further transformed in the following Corollary.

**Corollary 4.** In an interference-limited scenario with  $\alpha = 4$ ,  $R_1$  and  $R_2$  are given by

$$\tilde{R}_1 = \frac{1}{\ln(2)} \sum_{i=0}^{\hat{\kappa}_s-1} \frac{(-1)^i}{i!} \left[ \frac{\partial^i}{\partial s^i} V^+(s) \right]_{s=1} \quad (56a)$$

$$\tilde{R}_2 = \frac{1}{\ln(2)} ((\pi - 2\text{Si}(V_2(s))) \sin(V_2(s)) - 2\text{Ci}(V_2(s)) \cos(V_2(s))) \quad (56b)$$

where

$$V^+(s) = (\pi - 2\text{Si}(V_1(s))) \sin(V_1(s)) - 2\text{Ci}(V_1(s)) \cos(V_1(s)), \quad (57a)$$

$$V_1(s) = \frac{\pi^2}{2} \lambda_t \left( p \left( \frac{e_1}{\omega_s} s \right)^{\frac{1}{2}} + (1-p) \left( \frac{C_d}{\omega_s} s \right)^{\frac{1}{2}} \right), \quad (57b)$$

$$V_2(s) = \frac{\pi^2}{2} \lambda_t \left( p \left( \frac{e_1}{\eta_{g,0}} \right)^{\frac{1}{2}} + (1-p) \left( \frac{C_d}{\eta_{g,0}} \right)^{\frac{1}{2}} \right). \quad (57c)$$

*Proof:* It can be proved by using the interchangeable property of differentiation and integration.  $\square$

**Corollary 5.** For the nearest association strategy, the average achievable rate of  $U_0$  is given by

$$R_{c,n} = \frac{1}{\ln(2)} \int_0^\infty \frac{P_{c,n}(\bar{\gamma})}{1+\bar{\gamma}} d\bar{\gamma}, \quad (58)$$

where  $P_{c,n}(\bar{\gamma})$  is defined in Proposition 5.

**Corollary 6.** For the nearest association strategy, the average achievable rate of  $U_0$  in the interference-limited scenario is given by

$$\tilde{R}_{c,n} = \frac{1}{\ln(2)} \int_0^\infty \frac{\tilde{P}_{c,n}(x)}{1+x} dx, \quad (59)$$

where  $\tilde{P}_{c,n}(x)$  is defined in Proposition 6.

## VI. NUMERICAL RESULTS

In this section, we present numerical results to validate the effectiveness of the above analysis, including the approximate signal power distribution, coverage probability and average achievable rate. We also explore several insights regarding the impacts of different system parameters on the communication performance.

### A. Simulation Setup

Unless otherwise mentioned, the parameters of the Monte Carlo (MC) simulations are listed as follows. The GPP for the distribution of TXs and RISs is generated in a disk area of radius 5000 m. The path loss per unit distance of the direct link and the reflected path are given by  $C_d = C_r = -30$  dB.  $U_0$  is located at the origin. The AWGN power is  $\sigma_0^2 = -70$  dBm. Similar simulation parameters setting has been applied in [29], [35].

### B. Analysis of Approximate Distributions

The accuracy of approximating the received signal power  $S_0^+$  as a gamma random variable is verified here. The path loss exponent is set to be  $\alpha = 2.5$ . The locations of  $U_0$ 's corresponding TX and RIS are respectively assumed to be fixed with the coordinates (20, 0) and (20, 3), similarly as in [39]. The shape parameters of the Nakagami- $m$  distribution<sup>5</sup> vary in  $m_h, m_r \in \{1, 2, 4\}$ , and the number of elements varies in  $N \in \{16, 32, 64\}$ . Fig. 2 illustrates the CCDF of  $S_0^+$  with different numbers of elements and different shape parameters. The proposed fitting method based on a gamma distribution matches very well with the simulation results. It can be observed that increasing the number of elements can significantly improve the channel power gain. For example, when  $m_h = m_r = 1$  and  $\bar{F}_{S_0^+}(x) = 0.8$ , we can see that  $x = -52$  dB and  $x = -41$  dB for  $N = 16$  and  $N = 64$ , respectively.

We also investigate the approximation of the interference power from an interfering TX with an assisting RIS,  $I_{1,k}$ . The coordinates of the interfering TX and its corresponding RIS are also (0, 20) and (3, 20), respectively. The shape parameter of the Nakagami- $m$  distribution will not affect the interference distribution due to the lack of reflect beamforming. Fig. 3 gives the CCDF of  $I_{1,k}$  with different numbers of elements. Compared with the case with reflect beamforming in Fig. 2, the interference power is much smaller even if the interfering TX without beamforming is at the same distance from  $U_0$  as the associated TX. Another important point is that the interference power will not grow as rapidly with the increase of the elements as the case with reflect beamforming. This shows that using RIS with a large number of elements can significantly increase the received SINR in a multi-cell network.

### C. Fixed Association Strategy Analysis

Fig. 4 illustrates the coverage probability versus the transmit power with different densities of TXs.  $U_0$  is associated with a fixed TX that has an assisting RIS. The path loss exponent is  $\alpha = 2.5$ . The number of elements of each RIS is  $N = 32$ , and the RIS association probability is  $p = 0.5$ . The Nakagami- $m$  shape parameters are set to be  $m_h = m_r = 2$ . The distance between a RIS and its corresponding TX varies in  $d_0 \in \{3, 5\}$ . The location of  $U_0$ 's corresponding TX is fixed

<sup>5</sup>For clarity, we use  $m_h = m_r$  in simulations. However,  $m_h$  and  $m_r$  can be set arbitrarily and independently.

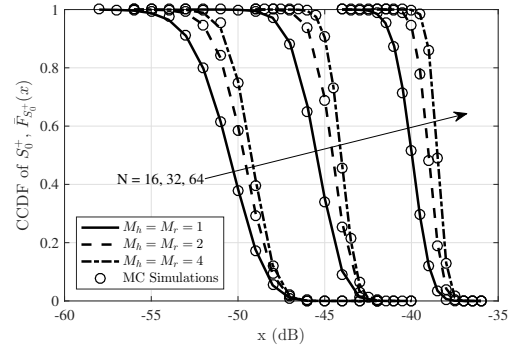


Fig. 2. Approximate CCDF of  $S_0^+$  and simulation results.

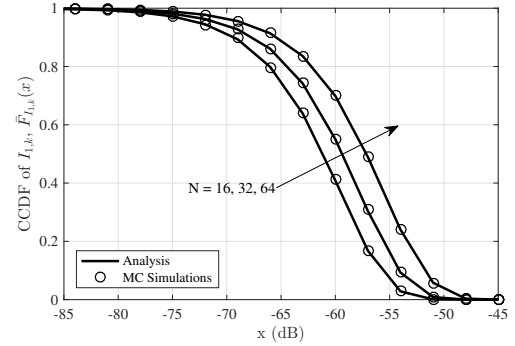


Fig. 3. Approximate CCDF of  $I_{1,k}$  and simulation results.

at (20, 0), while the locations of its assisting RIS are (20, 3) and (20, 5) for  $d_0 = 3$  and  $d_0 = 5$ , respectively. To illustrate the impact of interfering TXs, the coverage probability curve without interfering TXs, labelled as 'No Interference', is also given for  $d_0 = 3$ . We can see that, even though several approximations are applied to obtain the closed form coverage probability in Proposition 3, the proposed analytical result is still accurate for a large density of TXs, e.g.,  $\lambda_t = 10^{-3}$ . Interfering TXs sharing the same resource block will always deteriorate the system performance, but the influence is only significant when the density of TXs is large. For example, when the transmit power is  $P = -24$  dBm and  $d_0 = 3$ , the coverage probability is 0.53 and 0.93 for  $\lambda_t = 10^{-3}$  and  $\lambda_t = 10^{-4}$ , respectively. However, the impact of interfering TXs is negligible when  $\lambda_t < 10^{-4}$  as the curves are close to the ideal case without interference. Further, it can be observed that increasing the distance between TX and its associating RIS has negative impact on the system performance due to the double fading effect of RIS assisted transmission. Increasing  $d_0$  will lead to lower desired signal power received at  $U_0$ .

Fig. 5 shows the coverage probability versus the transmit power when  $U_0$  is associated with a fixed TX without an assisting RIS.  $d_0 = 3$ . To illustrate the impact of path loss exponent on the system performance, the path loss exponent varies in  $\alpha \in \{2.5, 3, 3.5, 4\}$  for  $\lambda_t = 10^{-5}$ . The performance degradation due to interfering TXs is negligible if  $\lambda_t < 10^{-6}$ . Compared with Fig. 4, we can learn that associating  $U_0$  with

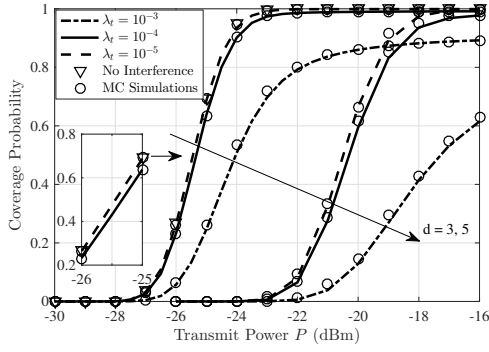


Fig. 4. Coverage probability versus transmit power with different densities of TXs. Fixed association strategy with assisting RIS.

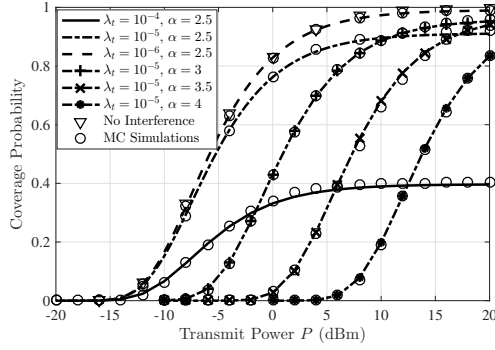


Fig. 5. Coverage probability versus transmit power with different densities of TXs. Fixed association strategy without assisting RIS.

a TX that has an assisting RIS can significantly improve the performance. For example, if  $\lambda_t = 10^{-5}$  and  $\alpha = 2.5$ , achieving the coverage probability of 0.9 requires the transmit power of  $P = -24$  dBm and 10 dBm for the cases with and without assisting RIS, respectively.

The impact of the RIS association probability  $p$  is explored in Fig. 6.  $U_0$  is associated with a fixed TX with an assisting RIS. The path loss exponent is  $\alpha = 2.5$ , and  $d_0 = 3$ . The RIS association probability and the number of elements vary in  $p \in \{0, 0.5, 1\}$  and  $N \in \{32, 64\}$ , respectively. As expected, increasing  $p$  will lead to lower coverage probability if the fixed associations strategy is applied since the interference power scattered by RISs is enhanced.

Fig. 7 shows the average achievable rate versus the transmit power with different densities of TXs.  $U_0$  is connected with a fixed TX that has an assisting RIS. Similar to the setup in Fig. 4, the distance between a RIS and its corresponding TX lies in  $d_0 \in \{3, 5\}$ . The RIS association probability and the path loss exponent are respectively  $p = 0.5$  and  $\alpha = 2.5$ , and the number of elements per RIS is  $N = 32$ . The density of TXs varies in  $\lambda_t \in \{10^{-6}, 10^{-5}, 10^{-4}\}$ . As expected, increasing the transmit power and reducing the density of TXs will lead to better performance of  $U_0$ . Similar to result regarding the coverage probability, the larger distance between TX and its connected RIS results in the lower average achievable rate due to the double fading effect.

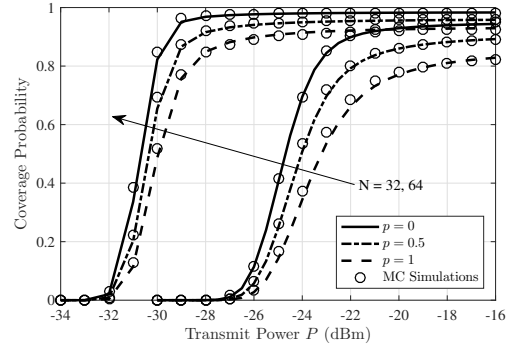


Fig. 6. Coverage probability versus transmit power with different RIS association probabilities. Fixed association strategy with assisting RIS.

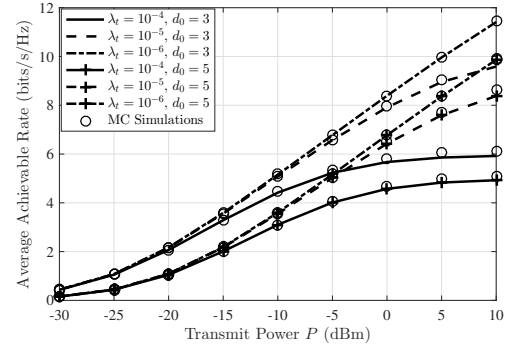


Fig. 7. Average achievable versus transmit power with different densities of TXs. Fixed association strategy.

#### D. Nearest Association Strategy Analysis

Fig. 8 illustrates the coverage probability against the transmit power when  $U_0$  is associated with the nearest TX and  $\alpha = 2.5$ . The density of TXs varies in  $\lambda_t \in \{10^{-5}, 5 \times 10^{-5}, 10^{-4}, 10^{-3}\}$ , and the RIS association probability is  $p = 0.9$ . The number of elements per RIS is  $N = 32$ , and the distance between TX and its connected RIS is  $d_0 = 3$ . To verify the analysis in Corollary 2, the curves for  $\alpha = 4$  are also given for  $\lambda_t = 10^{-4}$ . Increasing the density of TXs is beneficial for  $U_0$  within certain transmit power regime, since  $U_0$  is more likely to be connected with a closer TX with the nearest association strategy. Furthermore, we can observe that the coverage probability is independent with the density of TXs when the noise power is negligible, which proves our analysis in Remark 6. As a step further, we investigate the impact of the RIS association probability  $p$  on the average achievable rate and the coverage probability in the interference-limited scenario, i.e.,  $\gamma_t \rightarrow \infty$ , with the nearest association strategy in Fig. 9. The path loss exponent lies in  $\alpha \in \{2.5, 4\}$ . In the current simulation setup, it turns out that increasing the RIS association probability can also improve the system performance since  $U_0$  is more likely to be served by a RIS-assisted TX.

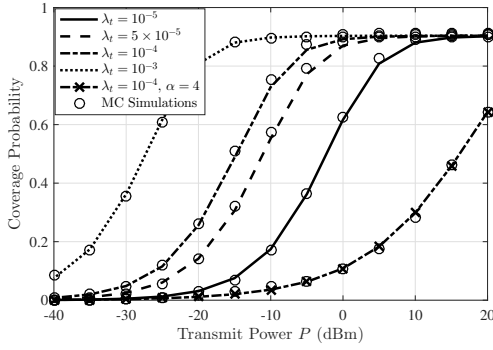


Fig. 8. Coverage probability versus transmit power with different densities of TXs. Nearest association strategy.

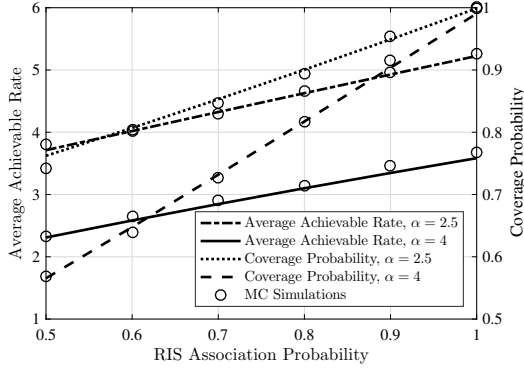


Fig. 9. Average achievable rate and coverage probability versus RIS association probability. Nearest association strategy.

## VII. CONCLUSIONS

This paper proposed a RIS-assisted multi-cell network with large-scale randomly deployed TXs, RISs and UEs. The locations of TXs and RISs were modeled by a GPP. We investigated the coverage probability and the average achievable rate of the typical user. The analytical results showed that increasing the density of TXs has no influence on the coverage probability and the average achievable rate in the large transmit SNR regime with the nearest association strategy. The analysis was validated by the numerical results, which also demonstrated the significant performance gain brought by the RIS assisted transmission with passive beamforming, and illustrated that increasing the density of TXs and the RIS association probability was detrimental and beneficial for the system performance with fixed and nearest association strategies, respectively.

## APPENDIX A

Since  $S_0^+$  is approximated by a gamma random variable with shape and scale parameters  $\kappa_s$  and  $\omega_s$ , we can have

$$\nu_s^2 = \frac{1}{\kappa_s} = \frac{\chi_2 - \chi_1^2}{\chi_1^2}. \quad (\text{A.1})$$

By using the multinomial theorem, it can be proved that  $\chi_2 - \chi_1^2$  and  $\chi_1^2$  can be given in polynomials as

$$\chi_2 - \chi_1^2 = a_0 + a_1 N + a_2 N^2 + a_3 N^3, \quad (\text{A.2a})$$

$$\chi_1^2 = a'_0 + a'_1 N + a'_2 N^2 + a'_3 N^3 + a'_4 N^4, \quad (\text{A.2b})$$

where  $a_i, i \in \{0, 1, 2, 3\}$  and  $a'_i, i \in \{0, 1, 2, 3, 4\}$  are some real coefficients. Therefore, we can have

$$\frac{1}{\kappa_s} \sim \frac{a_3}{a'_4 N}, \quad N \rightarrow \infty. \quad (\text{A.3})$$

## APPENDIX B

The Laplace transform of the interference power  $I$  with the fixed association strategy can be written as

$$\begin{aligned} \mathcal{L}_{I,f}(s) &= \mathbb{E}[e^{-sI}] \quad (\text{B.1}) \\ &= \mathbb{E}\left[\exp\left(-s\left(\sum_{k \in \Lambda_t \setminus \{0\}} I_{1,k} b_k + I_{2,k}(1-b_k)\right)\right)\right] \\ &\stackrel{(a)}{=} \mathbb{E}\left[\prod_{k \in \Lambda_t \setminus \{0\}} (p \exp(-sI_{1,k}) + (1-p) \exp(-sI_{2,k}))\right] \\ &\stackrel{(b)}{=} \mathbb{E}\left[\prod_{k \in \Lambda_t \setminus \{0\}} \left(\frac{p}{1 + (\eta_{g,k} + N\eta_{h,k})s} + \frac{1-p}{1 + \eta_{g,k}s}\right)\right], \\ &\stackrel{(c)}{\approx} \mathbb{E}\left[\prod_{k \in \Lambda_t \setminus \{0\}} \left(\frac{p}{1 + e_1 d_{g,k}^{-\alpha} s} + \frac{1-p}{1 + C_d d_{g,k}^{-\alpha} s}\right)\right] \\ &\stackrel{(d)}{=} \exp\left(2\pi\lambda_t \int_0^\infty \left(\frac{p}{1 + s e_1 r^{-\alpha}} + \frac{1-p}{1 + s C_d r^{-\alpha}} - 1\right) r dr\right) \\ &= \exp\left(2\pi\lambda_t p \int_0^\infty \left(\frac{1}{1 + s e_1 r^{-\alpha}} - 1\right) r dr\right) \\ &\quad \times \exp\left(2\pi\lambda_t (1-p) \int_0^\infty \left(\frac{1}{1 + s C_d r^{-\alpha}} - 1\right) r dr\right), \end{aligned}$$

where (a) follows from Lemma 2 in [30]; (b) is obtained by the fact that  $I_{1,k}$  and  $I_{2,k}$  both follow the exponential distribution. From the Slivnyak's theorem, conditioning on a TX at a fixed location does not influence the distribution of other clusters; (c) is due to the distance approximation. Considering the spatial correlation between the locations of a TX and its associated RIS where a separate link is required to pass the CSI,  $d_{g,j}$  can be significantly larger than  $d_0$ . A similar assumption is also applied in [27]. Besides, (d) holds by using the probability generating functional (PGFL). Thus, the result in Proposition 1 can be obtained.

## APPENDIX C

We have used the moment matching approach to fit the distribution of  $S_0^+$  to a gamma random variable with shape

parameter  $\kappa_s$  and scale parameter  $\omega_s$  in Sec.III. Here, we round  $\kappa_s$  to its nearest integer  $\hat{\kappa}_s$ . Then, we can have

$$\begin{aligned} P_1(\bar{\gamma}) &= \mathbb{P}(\gamma_0^+ > \bar{\gamma}) \\ &= \mathbb{P}(S_0^+ > \bar{\gamma}(I + \gamma_t^{-1})) \\ &= \mathbb{E}_I [\bar{F}_{S_0^+}(\bar{\gamma}(I + \gamma_t^{-1}))] \\ &= \mathbb{E}_X \left[ \frac{\Gamma(\hat{\kappa}_s, X)}{\Gamma(\hat{\kappa}_s)} \right], \end{aligned} \quad (\text{C.1})$$

where

$$X = \frac{\bar{\gamma}}{\omega_s} (I + \gamma_t^{-1}). \quad (\text{C.2})$$

Since  $\hat{\kappa}_s$  is an integer, using the series expansion of the upper incomplete gamma function, we can write

$$\begin{aligned} P_1(\bar{\gamma}) &= \sum_{i=0}^{\hat{\kappa}_s-1} \frac{(-1)^i}{i!} \mathbb{E}_X [(-1)^i X^i e^{-X}] \\ &= \sum_{i=0}^{\hat{\kappa}_s-1} \frac{(-1)^i}{i!} \mathbb{E}_X \left[ \left[ \frac{\partial^i}{\partial s^i} e^{-sX} \right]_{s=1} \right] \\ &\stackrel{(a)}{=} \sum_{i=0}^{\hat{\kappa}_s-1} \frac{(-1)^i}{i!} \left[ \frac{\partial^i}{\partial s^i} \mathbb{E}_X [e^{-sX}] \right]_{s=1} \\ &= \sum_{i=0}^{\hat{\kappa}_s-1} \frac{(-1)^i}{i!} \left[ \frac{\partial^i}{\partial s^i} \mathcal{L}_X(s) \right]_{s=1}, \end{aligned} \quad (\text{C.3})$$

where (a) follows by interchanging differentiation and expectation.

The Laplace transform of  $X$  can be derived directly from the Laplace transform of  $I$ :

$$\begin{aligned} \mathcal{L}_X(s) &= \mathbb{E}_I \left[ \exp \left( -\frac{s\bar{\gamma}}{\omega_s} (I + \gamma_t^{-1}) \right) \right] \\ &= \exp \left( -\frac{s\bar{\gamma}}{\omega_s} \gamma_t^{-1} \right) \mathcal{L}_{I,f} \left( \frac{s\bar{\gamma}}{\omega_s} \right). \end{aligned} \quad (\text{C.4})$$

Using the result in Proposition 1, we arrive at the expression of  $P_1$  given in the proposition.

#### APPENDIX D

Since  $S_0^*$  is exponentially distributed, we can write

$$\begin{aligned} P_2 &= \mathbb{P}(\gamma_0^* > \bar{\gamma}) \\ &= \mathbb{P}(S_0^* > \bar{\gamma}(I + \gamma_t^{-1})) \\ &= \mathbb{E}_I [\bar{F}_{S_0^*}(\bar{\gamma}(I + \gamma_t^{-1}))] \\ &= \mathbb{E}_I \left[ \exp \left( -\frac{\bar{\gamma}}{\eta_{g,0}} (I + \gamma_t^{-1}) \right) \right] \\ &= \exp \left( -\frac{\bar{\gamma}}{\eta_{g,0}} \gamma_t^{-1} \right) \mathcal{L}_{I,f} \left( \frac{\bar{\gamma}}{\eta_{g,0}} \right). \end{aligned} \quad (\text{D.1})$$

Thus, the proof is complete.

#### APPENDIX E

The coverage probability of  $U_0$  can be transformed as

$$\begin{aligned} P_{c,n}(\bar{\gamma}) &= \mathbb{E}_{d_{g,0}} [\mathbb{P}(\gamma_0 > \bar{\gamma})] \\ &= \mathbb{E}_{d_{g,0}} [p\mathbb{P}(\gamma_0^+ > \bar{\gamma}) + (1-p)\mathbb{P}(\gamma_0^* > \bar{\gamma})] \\ &= p \int_0^\infty \mathbb{P}(\gamma_0^+ > \bar{\gamma}) f_{d_{g,0}}(r) dr \\ &\quad + (1-p) \int_0^\infty \mathbb{P}(\gamma_0^* > \bar{\gamma}) f_{d_{g,0}}(r) dr. \end{aligned} \quad (\text{E.1})$$

The distance approximation used in the proof of Proposition 1 such that  $d_{g,j} \approx d_{r,j}$ ,  $j \in \Lambda_2^{(P)}$  is applied here. Then, following a similar procedure to Proposition 3 and Proposition 4, using the result in Proposition 2, and recalling the definitions of  $\omega_s$  and  $\eta_{g,0}$ , we can directly derive  $\mathbb{P}(\gamma_0^+ > \bar{\gamma})$  and  $\mathbb{P}(\gamma_0^* > \bar{\gamma})$  as  $q^+(r)$  and  $q^*(r)$ , respectively.

#### APPENDIX F

As defined in (19), the average achievable rate of the typical user can be rewritten as

$$\begin{aligned} R &\stackrel{(a)}{=} \int_0^\infty \log_2(1 + \bar{\gamma}) \frac{\partial(1 - P_c(\bar{\gamma}))}{\partial \bar{\gamma}} d\bar{\gamma} \\ &= -\frac{1}{\ln(2)} \int_0^\infty \int_0^{\bar{\gamma}} \frac{1}{1+x} dx \frac{\partial P_c(\bar{\gamma})}{\partial \bar{\gamma}} d\bar{\gamma} \\ &\stackrel{(b)}{=} -\frac{1}{\ln(2)} \int_0^\infty \frac{1}{1+x} \int_x^\infty \frac{\partial P_c(\bar{\gamma})}{\partial \bar{\gamma}} d\bar{\gamma} dx \\ &= \frac{1}{\ln(2)} \int_0^\infty \frac{P_c(x)}{1+x} dx, \end{aligned} \quad (\text{F.1})$$

where (a) is due to the mathematical relationship between the PDF and CDF; (b) is obtained by changing the integration order.

#### REFERENCES

- [1] W. Jiang, B. Han *et al.*, "The road towards 6G: A comprehensive survey," *IEEE Open J. Commun. Soc.*, vol. 2, pp. 334–366, 2021.
- [2] S. Dang, O. Amin *et al.*, "What should 6G be?" *Nat. Electron.*, vol. 3, no. 1, pp. 20–29, 2020.
- [3] W. Tang, M. Z. Chen *et al.*, "Wireless communications with reconfigurable intelligent surface: Path loss modeling and experimental measurement," *IEEE Trans. Wireless Commun.*, vol. 20, no. 1, pp. 421–439, 2020.
- [4] Q. Wu and R. Zhang, "Towards smart and reconfigurable environment: Intelligent reflecting surface aided wireless network," *IEEE Commun. Mag.*, vol. 58, no. 1, pp. 106–112, 2020.
- [5] Q. Wu, S. Zhang *et al.*, "Intelligent reflecting surface-aided wireless communications: A tutorial," *IEEE Trans. Commun.*, vol. 69, no. 5, pp. 3313–3351, 2021.
- [6] C. Huang, A. Zappone *et al.*, "Reconfigurable intelligent surfaces for energy efficiency in wireless communication," *IEEE Trans. Wireless Commun.*, vol. 18, no. 8, pp. 4157–4170, 2019.
- [7] P. Xu, G. Chen *et al.*, "Ergodic secrecy rate of RIS-assisted communication systems in the presence of discrete phase shifts and multiple eavesdroppers," *IEEE Wireless Commun. Lett.*, vol. 10, no. 3, pp. 629–633, 2021.
- [8] C. Pan, H. Ren *et al.*, "Reconfigurable intelligent surfaces for 6G systems: Principles, applications, and research directions," *IEEE Commun. Mag.*, vol. 59, no. 6, pp. 14–20, 2021.
- [9] X. Pang, N. Zhao *et al.*, "IRS-assisted secure UAV transmission via joint trajectory and beamforming design," *IEEE Trans. Commun.*, vol. 70, no. 2, pp. 1140–1152, 2022.

- [10] X. Pang, M. Sheng *et al.*, "When UAV meets IRS: Expanding air-ground networks via passive reflection," *IEEE Wireless Commun.*, vol. 28, no. 5, pp. 164–170, 2021.
- [11] Ö. Özdoğan, E. Björnson, and E. G. Larsson, "Intelligent reflecting surfaces: Physics, propagation, and pathloss modeling," *IEEE Wireless Commun. Lett.*, vol. 9, no. 5, pp. 581–585, 2019.
- [12] E. Basar, M. Di Renzo *et al.*, "Wireless communications through reconfigurable intelligent surfaces," *IEEE Access*, vol. 7, pp. 116 753–116 773, 2019.
- [13] M. Badiu and J. P. Coon, "Communication through a large reflecting surface with phase errors," *IEEE Wireless Commun. Lett.*, vol. 9, no. 2, pp. 184–188, 2020.
- [14] T. Wang, G. Chen *et al.*, "Chernoff bound and saddlepoint approximation for outage probability in IRS-assisted wireless systems," in *Proc. IEEE Global Commun. Conf. Wkshps. (GC Wkshps)*, Madrid, Spain, Dec. 2021, pp. 1–5.
- [15] S. Atapattu, R. Fan *et al.*, "Reconfigurable intelligent surface assisted two-way communications: Performance analysis and optimization," *IEEE Trans. Wireless Commun.*, vol. 68, no. 10, pp. 6552–6567, 2020.
- [16] Z. Cui, K. Guan *et al.*, "SNR coverage probability analysis of RIS-aided communication systems," *IEEE Trans. Veh. Technol.*, vol. 70, no. 4, pp. 3914–3919, 2021.
- [17] T. Wang, G. Chen *et al.*, "Study of intelligent reflective surface assisted communications with one-bit phase adjustments," in *Proc. IEEE Global Commun. Conf. (GLOBECOM)*, Virtual, Dec. 2020, pp. 1–6.
- [18] H. Ibrahim, H. Tabassum, and U. T. Nguyen, "Exact coverage analysis of intelligent reflecting surfaces with Nakagami-m channels," *IEEE Trans. Veh. Technol.*, vol. 70, no. 1, pp. 1072–1076, 2021.
- [19] S. A. Tegos, D. Tyrovolas *et al.*, "On the distribution of the sum of double-Nakagami-m random vectors and application in randomly reconfigurable surfaces," *IEEE Trans. Veh. Technol.*, 2022, Early Access.
- [20] T. Van Chien, A. K. Papazafeiropoulos *et al.*, "Outage probability analysis of IRS-assisted systems under spatially correlated channels," *IEEE Wireless Commun. Lett.*, vol. 10, no. 8, pp. 1815–1819, 2021.
- [21] T. Wang, M.-A. Badiu *et al.*, "Outage probability analysis of STAR-RIS assisted NOMA network with correlated channels," *IEEE Commun. Lett.*, 2022, Early Access.
- [22] M. Haenggi, *Stochastic geometry for wireless networks*. Cambridge University Press, 2012.
- [23] G. Chen, J. P. Coon, and M. Di Renzo, "Secrecy outage analysis for downlink transmissions in the presence of randomly located eavesdroppers," *IEEE Trans. Inf. Forensics Security*, vol. 12, no. 5, pp. 1195–1206, 2017.
- [24] M. Nemati, J. Park, and J. Choi, "RIS-assisted coverage enhancement in millimeter-wave cellular networks," *IEEE Access*, vol. 8, pp. 188 171–188 185, 2020.
- [25] M. A. Kishk and M.-S. Alouini, "Exploiting randomly located blockages for large-scale deployment of intelligent surfaces," *IEEE J. Sel. Areas Commun.*, vol. 39, no. 4, pp. 1043–1056, 2020.
- [26] Y. Zhu, G. Zheng, and K.-K. Wong, "Stochastic geometry analysis of large intelligent surface-assisted millimeter wave networks," *IEEE J. Sel. Areas Commun.*, vol. 38, no. 8, pp. 1749–1762, 2020.
- [27] J. Lyu and R. Zhang, "Hybrid active/passive wireless network aided by intelligent reflecting surface: System modeling and performance analysis," *IEEE Trans. Wireless Commun.*, vol. 20, no. 11, pp. 7196–7212, 2021.
- [28] C. Zhang, W. Yi *et al.*, "Reconfigurable intelligent surfaces aided multi-cell NOMA networks: A stochastic geometry model," *IEEE Trans. Commun.*, vol. 70, no. 2, pp. 951–966, 2022.
- [29] T. Shafique, H. Tabassum, and E. Hossain, "Stochastic geometry analysis of IRS-assisted downlink cellular networks," *IEEE Trans. Commun.*, vol. 70, no. 2, pp. 1442–1456, 2022.
- [30] A. Guo, Y. Zhong *et al.*, "The Gauss–Poisson process for wireless networks and the benefits of cooperation," *IEEE Trans. Commun.*, vol. 64, no. 5, pp. 1916–1929, 2016.
- [31] N. Deng and M. Haenggi, "The benefits of hybrid caching in Gauss–Poisson D2D networks," *IEEE J. Sel. Areas Commun.*, vol. 36, no. 6, pp. 1217–1230, 2018.
- [32] T. Wang, M.-A. Badiu *et al.*, "Outage probability analysis of RIS-assisted wireless networks with Von Mises phase errors," *IEEE Wireless Commun. Lett.*, vol. 10, no. 12, pp. 2737–2741, 2021.
- [33] Q. Wu and R. Zhang, "Beamforming optimization for wireless network aided by intelligent reflecting surface with discrete phase shifts," *IEEE Tran. Commun.*, vol. 68, no. 3, pp. 1838–1851, 2019.
- [34] T. Wang, M.-A. Badiu *et al.*, "Performance analysis of IOS-assisted NOMA system with channel correlation and phase errors," *IEEE Trans. Veh. Technol.*, Early Access, 2022.
- [35] Z. Xie, W. Yi *et al.*, "STAR-RIS aided NOMA in multi-cell networks: A general analytical framework with gamma distributed channel modeling," *IEEE Trans. Commun.*, 2022, Early Access.
- [36] T. Hou, Y. Liu *et al.*, "MIMO assisted networks relying on intelligent reflective surfaces: A stochastic geometry based analysis," *IEEE Trans. Veh. Technol.*, vol. 71, no. 1, pp. 571–582, 2021.
- [37] Z. Xie, W. Yi *et al.*, "Modeling and coverage analysis for RIS-aided NOMA transmissions in heterogeneous networks," 2020. [Online]. Available: <https://arxiv.org/abs/2104.13182>.
- [38] A. Goldsmith, *Wireless communications*. Cambridge university press, 2005.
- [39] Q. Wu and R. Zhang, "Intelligent reflecting surface enhanced wireless network via joint active and passive beamforming," *IEEE Trans. Wireless Commun.*, vol. 18, no. 11, pp. 5394–5409, 2019.



**Tianxiong Wang** received the B.Sc. degree in electronic science and technology from the Beijing Institute of Technology, China, in 2019. He is currently pursuing the D.Phil. degree with the Department of Engineering Science, University of Oxford, U.K. His research interests are in the fields of reconfigurable intelligent surface (RIS), performance analysis, non-orthogonal multiple access (NOMA), stochastic geometry, and wireless communications. He serves as a reviewer for the IEEE COMMUNICATIONS LETTERS, IEEE WIRELESS COMMUNICATIONS LETTERS, and IEEE TRANSACTIONS ON WIRELESS COMMUNICATIONS.



**Mihai-Alin Badiu** received the Dipl.-Ing., M.S., and Ph.D. degrees in electrical engineering from the Technical University of Cluj-Napoca, Romania, in 2008, 2010, and 2012, respectively. From 2012 to 2019, he was a Post-Doctoral Researcher and an Assistant Professor with the Department of Electronic Systems, Aalborg University, Denmark. From 2016 to 2018, he held an Individual Post-Doctoral Fellowship from the Danish Council for Independent Research. He is currently a Post-Doctoral Research Assistant with the Department of Engineering Science and a Lecturer in Electrical Engineering at Balliol College, University of Oxford, U.K. His research interests include wireless networks theory, signal processing for communications, and probabilistic modeling and inference.



**Gaojie Chen** (S'09 – M'12 – SM'18) received the B.Eng. and B.Ec. Degrees in electrical information engineering and international economics and trade from Northwest University, China, in 2006, and the M.Sc. (Hons.) and PhD degrees in electrical and electronic engineering from Loughborough University, Loughborough, U.K., in 2008 and 2012, respectively. After graduation, he took up academic and research positions at DT Mobile, Loughborough University, University of Surrey, University of Oxford and University of Leicester, U.K. He

is currently an Assistant Professor with the Institute for Communication Systems, 5GIC & 6GIC, University of Surrey, U.K. His current research interests include information theory, wireless communications, satellite communications, cognitive radio, the Internet of Things, secrecy communications, and random geometric networks. He received the Exemplary Reviewer Awards of the IEEE WIRELESS COMMUNICATIONS LETTERS in 2018, the IEEE TRANSACTIONS ON COMMUNICATIONS in 2019 and the IEEE COMMUNICATIONS LETTERS in 2020 and 2021; and Exemplary Editor Awards of the IEEE COMMUNICATIONS LETTERS and IEEE WIRELESS COMMUNICATIONS LETTERS in 2021 and 2022, respectively. He serves as an Associate Editor for the IEEE COMMUNICATIONS LETTERS, IEEE WIRELESS COMMUNICATIONS LETTERS, IEEE JOURNAL ON SELECTED AREAS IN COMMUNICATIONS - MACHINE LEARNING IN COMMUNICATIONS AND NETWORKS and *Electronics Letters* (IET).



**Justin P. Coon** (Senior Member, IEEE) received the B.Sc. degree (with distinction) in electrical engineering from Calhoun Honours College, Clemson University, Clemson, SC, USA, in 2000 and the Ph.D. degree in communications from the University of Bristol, Bristol, U.K., in 2005. He held various research positions with Toshiba Research Europe Ltd. (TREL) from 2004 to 2013, including the position of a Research Manager from 2010 to 2013, during which, he led all research on physical layer communications and network science with

TREL. He was a Visiting Fellow with the School of Mathematics, University of Bristol, from 2010 to 2012, and was a Reader with the Department of Electrical and Electronic Engineering from 2012 to 2013. In 2013, he joined the University of Oxford, Oxford, U.K., where he is currently a Professor of Engineering Science and the Emmott Fellow in Engineering Science with Oriel College, Oxford, U.K. He has authored or coauthored more than 200 papers in IEEE and APS journals and conferences and is a named Inventor on more than 30 patents. He was the recipient of the Toshiba's Distinguished Research Award for his work on 4G systems and three best paper awards. He was the Editor of several IEEE journals and has Chaired or Co-chaired various conferences. He is a Fellow of the Institute for Mathematics and its Applications.